HHS Public Access

Author manuscript

Nat Genet. Author manuscript; available in PMC 2012 August 01.

Published in final edited form as:

Nat Genet. ; 44(2): 193–199. doi:10.1038/ng.1078.

CEP41 is mutated in Joubert syndrome and is required for tubulin glutamylation at the cilium

Ji Eun Lee[1], **Jennifer L. Silhavy**[1], **Maha S. Zaki**[2], **Jana Schroth**[1], **Stephanie L. Bielas**[1], **Sarah E. Marsh**[1], **Jesus Olvera**[1], **Francesco Brancati**[3,4], **Miriam Iannicelli**[3], **Koji Ikegami**[12], **Andrew M. Schlossman**[1], **Barry Merriman**[5], **Tania Attié-Bitach**[6], **Clare V. Logan**[7], **Ian A. Glass**[8], **Andrew Cluckey**[9], **Carrie M. Louie**[1], **Jeong Ho Lee**[1], **Hilary R. Raynes**[10], **Isabelle Rapin**[10], **Ignacio P. Castroviejo**[11], **Mitsutoshi Setou**[12], **Clara Barbot**[13], **Eugen Boltshauser**[14], **Stanley F. Nelson**[5], **Friedhelm Hildebrandt**[9], **Colin A. Johnson**[7], **Daniel A. Doherty**[8], **Enza Maria Valente**[3,15], and **Joseph G. Gleeson**[1]

[1]Neurogenetics Laboratory, Institute for Genomic Medicine, Department of Neurosciences and Pediatrics, Howard Hughes Medical Institute, University of California, San Diego, CA 92093, USA [2]Clinical Genetics Department, Human Genetics and Genome Research Division, National Research Centre, El-Tahrir St., Dokki, Giza, 12311 Cairo, Egypt [3]Casa Sollievo della Sofferenza Hospital, CSS-Mendel Laboratory, 71013 San Giovanni Rotondo (FG), Italy [4]Medical Genetics Unit, Department of Biopathology and Diagnostic Imaging, Tor Vergata University, 00133 Rome, Italy [5]Department of Human Genetics, Pathology and Laboratory Medicine, David Geffen School of Medicine, University of California, Los Angeles CA 90095, USA [6]Département de Génétique, INSERM U781, Hôpital Necker-Enfants Malades, Université Paris Descartes, Paris, France [7]Section of Ophthalmology and Neurosciences, Wellcome Trust Brenner Building, Leeds Institute of Molecular Medicine, St James's University Hospital, Leeds, LS9 7TF, UK [8]Divisions of Developmental Medicine and Genetic Medicine, Department of Pediatrics, University of Washington Seattle Children's Hospital, 4800 Sand Point Way NE, Seattle, WA 98105, USA [9]Department of Pediatrics and Communicable Diseases, Howard Hughes Medical Institute, University of Michigan, Ann Arbor, Michigan, USA [10]Saul R. Korey Department of Neurology, Department of Pediatrics, and Rose F. Kennedy Intellectual and Developmental Disabilities Research Center, Albert Einstein College of Medicine, Bronx, N. Y. 10461, USA [11]Pediatric Neurology Service, University Hospital La Paz, Paseo de la Castellana 261, Madrid 28046, Spain [12]Department of Cell Biology and Anatomy, Hamamatsu University School of Medicine, 1-20-1 Handayama, Hamamatsu 431-3192, Japan [13]Serviço de Neuropediatria, Hospital de Crianças Maria Pia, Rua da Boavista, 827, 4050-111 Porto, Portugal [14]Deparmtent of Pediatric Neurology,

Correspondence should be addressed to J.G.G. (jogleeson@ucsd.edu).

AUTHOR CONTRIBUTIONS

J.E.L. M.S.Z. and J.G.G. designed the study and experiments with substantial contributions from B.M. and S.F.N. helped fine mapping, J.L.S., S.L.B., J.O., F.B., M.I., A.M.S., T.A.-B., C.V.L., I.A.G., A.C., F.H., C.A.J., D.A.D., and E.M.V. performed genetic screening, and J.E.L., J.L.S., J.S., J.O., F.B., M.I., T.A.-B., I.A.G., D.A.D., C.M.L., and J.H.L. performed mutation analysis. M.S.Z., S.E.M., H.R.R., I.R., I.P.C., E.B. and E.M.V. identified and recruited patients, K.I. and M.S. shared critical reagents, and J.S. helped genotyping of mutant mice. J.E.L. performed microscopy, biochemical assays, zebrafish and mouse experiments. J.E.L. and J.G.G. interpreted the data and wrote the manuscript.

University Children's Hospital of Zürich, 75, CH 8032, Switzerland [15]Department of Medical and Surgical Pediatric Sciences, University of Messina, 98125 Messina, Italy

Abstract

Tubulin glutamylation is a post-translational modification (PTM) occurring predominantly on ciliary axonemal tubulin and has been suggested to be important for ciliary function [1,2]. However, its relationship to disorders of the primary cilium, termed 'ciliopathies', has not been explored. Here, in Joubert syndrome (JBTS) [3], we identify the JBTS15 locus and the responsible gene as *CEP41*, encoding a centrosomal protein of 41 KDa [4]. We show that CEP41 is localized to the basal body/primary cilium, and regulates the ciliary entry of TTLL6, an evolutionarily conserved polyglutamylase enzyme [5]. Depletion of *CEP41* causes ciliopathy-related phenotypes in zebrafish and mouse, and induces cilia axonemal glutamylation defects. Our data identify loss of *CEP41* as a cause of JBTS ciliopathy and highlight involvement of tubulin PTM in pathogenesis of the ciliopathy spectrum.

Joubert syndrome (OMIM 213300) is characterized by cerebellar hypoplasia, and neurological features including ataxia, psychomotor delay and oculomotor apraxia with a pathognomonic "molar tooth sign" on brain imaging. JBTS is frequently accompanied by various multiorgan signs and symptoms including retinal dystrophy, nephronophthisis, liver fibrosis and polydactyly, conditions associated with disorders of the ciliopathy spectrum of diseases that include Meckel-Gruber Syndrome (MKS), Bardet-Biedl Syndrome (BBS) and Nephronophthisis (NPHP). Though several causative genes have been found for these disorders, they account for less than 50% of cases [6,7]. We recruited a consanguineous two-branch Egyptian family (MTI-429) with five affected members (Fig. 1a–b, Table 1). We excluded linkage to previously identified JBTS loci using a panel of highly informative markers. Analysis of the family using whole genome Illumina 5K SNP Linkage chip Ver. IV scan identified a 5 Mbp region of linkage on chromosome 7q31.33–32.3, with a peak multipoint LOD score of 3.71, thus defining the JBTS15 locus. Haplotype analysis suggested a candidate interval between rs766240 and rs4728251 delineating the peak of highest significance (Supplementary Fig. 1a–b).

In order to further narrow the interval, we re-analyzed MTI-429 with the denser Affymetrix 250K NspI SNP array by applying a linkage-free IBD model [8]. The combination of the 5K SNP and 250K SNP linkage analyses generated a 2.8 Mbp IBD interval between rs17165226 and rs2971773 containing 26 genes (Fig. 1c). Direct sequence analyses of candidate genes within the interval led to the identification of a homozygous c.33+2T>G base change from reference sequence NM_018718, which was predicted to abolish the consensus splice donor site from exon 1 of the *CEP41* gene (Fig. 1d, Supplementary Fig. 2a). To confirm a mutation-specific splicing defect, we evaluated *CEP41* transcripts from MTI-429 primary patient fibroblasts (MTI-429-IV-1 and -IV-6). The RT-PCR result showed an absence of mature *CEP41* mRNA products in both affected patient cells, likely attributed to nonsense mediated decay (Fig. 1e).

We next screened an additional 832 ciliopathy patients: 720 of JBTS and 112 of MKS (many of whom were excluded for mutations in known ciliopathy genes) by directly sequencing *CEP41* and found two additional consanguineous families with homozygous mutations: c.97+3_5delGAG in an Egyptian JBTS family (MTI-1491) and c.423-2A>C in a Portuguese JBTS family (COR-98) (Fig. 1b–d, Supplementary Fig. 2a). These mutations were predicted to abolish the consensus splice donor site from exon 2 and the splice acceptor site from exon 7, respectively. Moreover, we confirmed that the mutation in MTI-1491 led to skipping of exon 2, thereby generating a premature stop in exon 3 (Supplementary Fig. 2b). Interestingly, in addition to the JBTS patients, the MTI-1491 family included one individual that was consistent with a phenotype of BBS and lacked the pathognomonic "molar tooth sign", and this patient was heterozygous for the c.97+3_5delGAG mutation (Supplementary Fig. 2b–d), suggesting *CEP41* may modify other ciliopathy conditions. From our cohort screen, we further identified heterozygous *CEP41* mutations (c.83C>A, c.107T>C, c.265C>G, c.536G>A, c.1078C>T), which altered highly conserved amino acid residues among vertebrates or led to a premature stop codon from five different families (Fig. 1d, Supplementary Fig. 2e, Supplementary Table 1). Each of these *CEP41*-mutated patients was additionally sequenced at the known JBTS genes, and in four there was an additional heterozygous potentially deleterious variant. It was notable that all homozygous mutations in *CEP41* were splice site mutations and identified only in JBTS patients while heterozygous variants were present in several ciliopathies including BBS and MKS. Our findings suggest that constitutive disruptions of *CEP41* result in JBTS, but that it may also serve as a modifier in the broader class of ciliopathies.

The *CEP41* gene has been poorly characterized except for its expression analysis in human organs including brain, testis and kidney [9]. *CEP41* encodes for Centrosomal Protein 41 KDa, predicted to contain two coiled-coils and a rhodanese-like domain (RHOD), which is structurally related to the catalytic subunit of the Cdc25 class of phosphatases [10]. However, we found that it lacks phosphatase activity in the *in vitro* para-Nitrophenylphosphate (pNPP) phosphatase assay (not shown). The RHOD domain therefore may be an enzymatically inactive version like some described RHOD domains in other proteins [10] functioning in protein interactions.

We next examined *CEP41* gene expression at the mRNA level and CEP41 protein subcellular localization. In zebrafish, *cep41* was expressed in the various ciliary organs including Kupffer's vesicle (KV), ear and heart as well as brain and kidney, regions predominantly affected in JBTS (Fig. 2a, Supplementary Fig. 3). In several ciliated cell lines such as mouse inner medullary collecting duct (IMCD3) cells and human retinal pigment epithelial (hTERT-RPE1) cells, endogenous CEP41 was predominantly noted at the centrioles and cilia (Fig. 2b). The cilia-associated expression/localization of *CEP41* prompted us to assess a possible role in cilia-related function. Accordingly, we performed knockdown experiments using translation blocking morpholino anti-sense oligonucleotides (MOs) in zebrafish. In *cep41* MOs-injected embryos (morphants), we observed peripheral heart edema and tail defects along with ciliopathy-related phenotypes including hydrocephalus, abnormal ear otolith formation and smaller eyes [11–14] (Supplementary Fig. 4a–b). We further found that injection of *cep41* MOs induced a decrease in production of the

protein with a dose-dependent phenotypic severity in the embryos (Supplementary Fig. 4b–c).

Cilia of KV, a structure that corresponds to the mammalian embryonic node, are essential to mediate lateral asymmetry [15]. Accordingly, the defect of left/right (L/R) asymmetry in the heart, a well-established ciliopathy phenotype in mammals, is also shown in zebrafish [16–18]. To examine whether *cep41* depletion results in the phenotype, we injected *cep41* MOs into Tg(*myl7:egfp*) zebrafish, a myocardium-specific transgenic reporter line, and found heart asymmetry defects such as inversion or failure to develop asymmetry of the ventricle and atrium (Fig. 2c). We also generated a *Cep41* knockout mouse line using a genetrap strategy (Supplementary Fig. 5a–c) and characterized its phenotype at E10–13. The homozygous $Cep41^{Gt/Gt}$ embryos showed a range of phenotypes: malformed hindbrain, exencephaly, brain hemorrhage, dilated pericardial sac and lethality as well as unexpected normal development in some homozygous mutants (Fig. 2d, Supplementary Fig. 5d–e, Supplementary Table 2). Although exencephaly, dilated heart and embryonic lethality suggest possible ciliary roles of *Cep41* in mouse [16,19,20], the phenotypic variability including normal development suggests the presence of extragenic phenotypic modifiers. We next investigated a genetic rescue using human *CEP41* in zebrafish *cep41* morphants, and found partial rescue of the cilia-associated morphant phenotype (Fig. 2e). The data suggest a potential evolutionarily conserved role of *CEP41* in ciliary function.

In order to explore possible roles of *CEP41*, we examined primary cultured fibroblasts of patients (MTI-429-IV-1 and -IV-6). We first tested whether *CEP41* mutant cells were devoid of CEP41 protein. Consistent with RT-PCR results (Fig. 1e), neither patient fibroblast line tested produced detectable CEP41, suggesting that these mutant cells are nearly null for CEP41 (Fig. 3a–b). In order to examine the effect of *CEP41* loss on cilia assembly, we induced ciliogenesis using serum starvation-mediated cell cycle arrest in confluent cells and visualized cilia by co-immunostaining using anti-ARL13B (cilia marker) [21] and GT335 (centrioles/cilia marker) [22] antibodies. In control fibroblasts, cilia were evident in 70 % of the total stained cells by 48 hr and 72 hr and nearly all co-stained with both markers (Fig. 3c, Supplementary Fig. 6). However, in the *CEP41* mutant fibroblasts, cilia were stained positively with ARL13B but not with GT335 (Fig. 3c). We quantified this effect and found that, whereas the percent of ARL13B-positive ciliated cells in the mutant fibroblasts was approximately equal to control fibroblasts, the percentage of GT335-positive ciliated cells was dramatically reduced in mutant fibroblasts (Supplementary Fig. 6). The GT335 antibody was originally generated to recognize the glutamylated forms (both mono- and polyglutamylation) of tubulin [23]. Therefore, the data suggest a potential role of *CEP41* in regulating tubulin glutamyl posttranslational modifications (PTMs).

Microtubules are the major structural scaffolds of the ciliary axoneme, composing the 9+0 or 9+2 arrangement, and undergo several PTMs including acetylation, detyrosination, glycylation and glutamylation (Supplementary Fig. 7). We therefore tested the effect of *CEP41* deficiency on these tubulin PTMs and found no significant defects other than glutamylation in *CEP41* mutant cells (Supplementary Fig. 8). In addition, the result of immunostaining using PolyE antibody (specific for polyglutamylated tubulins) in mutant

fibroblasts suggested that *CEP41* might function in regulating both tubulin mono- and polyglutamylation (Supplementary Fig. 9). Concurrently, we observed an effect of *cep41* deficiency on tubulin glutamylation as well as mildly reduced glycylation of the placode cilia in zebrafish (Fig. 3d, Supplementary Fig. 10). Forced expression of exogenous *CEP41* in the mutant fibroblasts remarkably increased the percentage of cells displaying glutamylated cilia (Fig. 3e), suggesting that glutamylation of the cilium is dependent on the expression of *CEP41*. Furthermore, we found that cell lines from patients with mutations in other JBTS genes including *TMEM216* and *INPP5E* displayed no such glutamylation defect (not shown), suggesting the phenotype of tubulin glutamylation phenotype is not a non-specific consequence of ciliopathy mutation. Together these data suggest that *CEP41* is required for ciliary glutamylation, but not necessary for initial cilia assembly.

Recent studies have shown that defective tubulin PTM is associated with altered ciliary axonemal structure [24–26]. Accordingly, we investigated whether the *CEP41*-dysfunctional cilia exhibiting glutamylation defects gave rise to abnormal axonemal structure. Transmission electron microscopy (TEM) analysis demonstrated that the depletion of *cep41* resulted in apparent structural defects in zebrafish renal cilia: specifically A tubules of the outer doublet microtubules of the axoneme were collapsed and/or duplicated (Fig. 3f, Supplementary Fig. 11). Previous studies have suggested that ciliary structural disruption affects ciliary motility [27,28], thus we examined the effect on the cilia of KV and kidney in zebrafish *cep41* morphants and found disabled motility of both cilia (Supplementary Fig. 12, Supplementary Mov. 1–6). Our data suggest that *CEP41* is involved in ciliary structural formation and motility by playing an essential role in tubulin glutamylation at the cilium.

We next investigated how *CEP41* modulates microtubule PTM at the ciliary axoneme. We noted that only microtubules of ciliary axonemes failed glutamylation, whereas those of centrioles were properly modified in *CEP41* mutant patient cells. (Fig. 3c). Furthermore, the lack of a Tubulin Tyrosine Ligase (TTL) domain in CEP41, requisite for enzyme activity [5], implied that it is unlikely to serve as a glutamylase. The main enzymes mediating tubulin glutamylation are members of the conserved TTL-like (TTLL) family [5]. Among several identified TTLL factors, we found consistently strong localization of TTLL6 at the basal body (the organizing structure at the base of cilium, derived from a mother centriole) and the cilium (Supplementary Fig. 13). In addition, previous studies have suggested that TTLL6 may be involved in ciliary function in several organisms including zebrafish [5,24,29]. We therefore examined the effects of *ttll6* deficiency using a *ttll6* translational blocking MO [30] in zebrafish and observed ciliopathy-related morphological phenotypes, similar to although less severe than what we observed following *cep41* knockdown (Fig. 4a). Additionally, *ttll6* morphants showed A-tubule axonemal defects, similar to those of *cep41* morphants (Fig. 4a), besides diverse axonemal structural defects, which were consistent with a previous report [30] (not shown). These data prompted us to test a possible functional relationship between *CEP41* and *TTLL6* by pair-wise co-immunoprecipitation (coIP), and found that the two proteins were part of a complex (Fig. 4b). Given evidence suggesting a candidate regulator associated with the transport of a polyglutamylase between the basal body and the cilium [29], we investigated a possible role for *CEP41* in TTLL6 localization. Following efficient knockdown of *Cep41* in IMCD cells using siRNA (Supplementary Fig. 14), we

found localization of TTLL6 restricted mainly to the basal bodies, suggesting a block of entry of TTLL6 into the cilium (Fig. 4c). These data suggest that *CEP41* functions in tubulin glutamylation by mediating transport of TTLL6 between the basal body and cilium.

Our finding of *CEP41* mutations in JBTS patients provides the first evidence directly linking defective tubulin glutamylation at the cilium to a cause of ciliopathies. Consistent with previous studies implicating tubulin PTMs in cilia function [23,24,31,32], our data suggest *CEP41*-mediated ciliary glutamylation is essential for axonemal formation. Moreover, we found that *CEP41* is required for transport of TTLL6 to modulate tubulin glutamylation, although it remains to be determined how these molecules co-function. Most likely, these proteins enter through the ciliary diffusion barrier at the transition zone [33,34] and are then transported along ciliary microtubules by intraflagellar transport (IFT) motor proteins. Thus examining whether CEP41 and TTLL6 form a complex with other factors at these locations will follow as a future study. Because tubulin glycylation is partially affected in *cep41* morphants and the phenotype of *cep41* morphants is more severe than *ttll6* morphants, it is likely that *CEP41* modulates other TTLL protein family members [5,30]. Evidence for this possibility has been described in recent studies suggesting involvement of both tubulin-glycylation and glutamylation, each regulated by different TTLL-family members, in maintaining ciliary structure and motility [30,35–37].

METHODS

Research subjects

MTI-429 family and additional families were recruited worldwide based upon the presence of at least one individual with a neuroradiographically proven ‘molar tooth sign’ associated with any JBTS or related disorder (JSRD) phenotype. Whenever possible, patients underwent a full diagnostic protocol as previously reported [38] and a standardized clinical questionnaire was obtained to assess extent of multi-organ involvement. We used standard methods to isolate genomic DNA from peripheral blood of the affected and unaffected family members after obtaining informed consent from all participating. Human subject research was approved by the Ethics Boards of Leeds (East), CASA Sollievo della Sofferenza Hospital/CSS-Mendel Institute, Hôpital Necker-Enfants Malades, Human subjects divisions at the University of Washington, University of Michigan Institutional Review Board and Human Research Protection Program, University of California, San Diego.

Genome-wide screen and fine mapping

A 5K whole genome linkage SNP-scan was performed with family MTI-429 using the Illumina Linkage IVb mapping panel [39], and analyzed with easyLinkage-Plus software [40], which runs Allegro version 1.2c in a PC Windows interface to calculate multipoint LOD scores. Parameters were set to autosomal recessive with full penetrance, and disease allele frequency of 0.001. Fine mapping on the pedigree was performed with the Affymetrix 250K *Nsp1* SNP array, and data were searched for common shared homozygous intervals from all affected family members using a custom script implemented in Mathematica (B. Merriman,

unpublished). This script identifies all homozygous intervals longer than 2 Mbp for which there are no more than 1 % heterozygous calls (to permit potential genotyping errors).

Mutation screening

Mutational screening of *CEP41* was performed by direct sequencing of the 11 coding exons and the adjacent intronic junctions in patients. PCR products obtained were treated with Exonuclease I (EXO) (Fermentas) and shrimp alkaline phosphatase (SAP) (Promega), and both strands were sequenced using a BigDye terminator cycle sequencing kit with an ABI3100 automated sequencer (Applied Biosystems). The primers and optimized PCR conditions used are depicted (Supplementary Table 3). Segregation of the identified mutations was investigated in all available family members. All identified mutations in *CEP41* were not encountered in 96 ethnically matched controls (188 chromosomes) upon direct sequencing.

Bioinformatics

Genetic location is according to the March 2006 Human Genome Browser build hg18. The ciliary proteome was searched using web-based tools [41,42]. Protein sequence conservation was determined using ClustalW multiple amino acid sequence alignment (see URL section).

Cloning

Full-length human *CEP41* was cloned into the TOPO blunt vector, and then shuttled into EGFP- and HA- containing vectors. Human and zebrafish *cep41* open reading frame were amplified by RT-PCR and cloned into the pCS2+ vector in order to synthesize RNA for injection into zebrafish embryos. Mouse *Cep41* open reading frame was amplified and cloned into the GST-, EGFP-, and FLAG-conjugated vectors for biochemical assays.

Generation of *Cep41* mutant mice

SIGTR ES cell line (AW0157), derived from 129P2/OlaHsd mice carrying a gene trap insertion [43] in the intron 1 of *Cep41*, was obtained from the European Conditional Mouse Mutagenesis Program (EUCOMM) and injected into C57BL/6 recipient blastocysts at the Mouse Biology Program, UC Davis. High-percentage chimeras (≥ 70 %) were bred to C57BL/6 for germline transmission. Gene-trapped mice were isolated by PCR for *β-galactosidase-neomycin* fusion gene and genotyped by Southern blot analysis hybridizing a ~10 kb (wild-type allele) and a ~8 kb (gene-trapped allele) product (Supplementary Fig. 5).

Zebrafish experiments

AB wild type zebrafish strains were used for *in situ* hybridization carried out by standard protocols using a DIG-labeled sense and anti-sense RNA probe for *cep41*. To knockdown zebrafish *cep41*, a translational blocking morpholino antisense oligonucleotide (MO, Gene Tools Inc) was used: 5′-CATCTTCCAGCAGCAGAGCTTCGGC-3′, diluted to appropriate concentrations in deionized sterile water, and injected into one-two cell stage embryos, obtained from natural spawning of zebrafish lines. To rescue the phenotypes in MO-injected embryos (morphants), RNA transcribed *in vitro* with the SP6 mMessage mMachine kit (Ambion) was co-injected. For characterization of ciliary defects in zebrafish embryos, the

morphological phenotype of either *cep41* or *ttll6* morphants were observed until 5 days post-fertilization (dpf) and quantified under bright-field microscopy based upon previously established criteria [44]. For western blot analysis at 1–2 dpf zebrafish control embryos and *cep41* morphants, about 50 embryos with each genotype were deyolked and the embryo lysates were extracted with RIPA buffer. For immunostaining with GT335, Ac-Tub and PolyG Abs in whole-mount zebrafish embryos, 3 dpf control embryos and *cep41* morphants were fixed in Dent's fixative (80 % MeOH: 20 % DMSO) at 4 °C overnight and incubated with GT335 Ab (1:400), Ac-Tub (1:400) and PolyG (1:300) as primary and with anti-goat-mouse 594 (1:1000) as secondary in diluted blocking solution (10 % normal goat serum: 0.5 % Tween 20 in PBS).

Cell culture and transfection

IMCD3, hTERT-RPE1, human fibroblast, and human embryonic kidney (HEK293) cells were grown in appropriate DMEM or MEM media supplemented with 10–20 % fetal bovine serum (FBS) at 37 °C in 5 % CO_2. Healthy human female and male control fibroblast cells were obtained from ATCC, and patient fibroblasts from skin biopsies were propagated in culture (≤ 5 passage number). Human fibroblast cells were transfected using the Basic Nucleofector Kit for Primary Mammalian Fibroblasts (Lonza). Other cells were transfected at 60–80 % confluency with plasmids or siRNAs using Lipofectamine 2000 (Invitrogen). The transfected cells were incubated for 24–72 hr with FBS or without FBS, dependent on the experimental purpose.

Fluorescence microscopy and transmission electron microscopy (TEM)

Images of immunofluorescent stained cells were obtained on a Deltavision RT Deconvolution microscope (Olympus IX70), under the same parameters for each experiment. Taken images were edited and analyzed using Adobe Photoshop CS. For electron microscopy, a standard protocol [45] was used except for one modification that tannic acid was included in the fixative to enhance the final contrast of the images. Formvar-coated slot grids (Electron microscopy Sciences) were used for sections (60–70 nm) to maximize visibility of the tissue and cross section performed to observe cilia axonemal structure.

Live imaging of zebrafish embryos

Zebrafish embryos (12 hpf for cilia in the KV and 2.5 dpf for the renal cilia) were transferred with embryo media to glass bottom culture dishes (MatTek), and 2.5 dpf embryos were anesthetized in tricaine solution (~0.016 mg/ml). Images were acquired for 30 sec – 2 min using a Perkin Elmer UltraView Vox Spinning Disk Confocal with EMCCD Hamamatsu 14 bit 1K × 1K camera, and edited with Volocity imaging software (Perkin Elmer).

Immunofluorescence and biochemical assay

For immunofluorescence, cells were fixed in 100 % methanol at −20 °C for 10 min. Primary antibodies used for immunofluorescence are: rabbit anti-CEP41, raised in rabbit to a purified bacterially expressed protein of GST-fused CEP41, (PRF&L, PA), mouse anti-acetylated-tubulin (Sigma), mouse GT335 Ab (gift from C. Janke), rabbit PolyE (gift from M.

Gorovsky) and rabbit anti-ARL13B (gift from T. Caspary). We used Alexa 488- or Alexa 594-conjugated secondary antibodies (Molecular Probes) and Hoechst 33342 nuclear dye. All antibodies were diluted in 4 % normal donkey serum in PBS, primary antibodies were incubated for overnight at 4 °C and secondary antibodies were applied for 1 hr at room temperature. For immunoblotting, cells were extracted with RIPA lysis buffer 3 days after transfection and boiled with SDS sample buffer. Same concentrations of lysates were loaded for paired experiments. Primary antibodies used for western blotting were: rabbit anti-GFP (Roche), mouse anti-Flag (Sigma), and mouse anti-alpha-Tubulin (Sigma). Bound antibodies were detected using horseradish peroxidase-conjugated secondary antibodies (Pierce). For co-immunoprecipitation (co-IP), whole cell extracts (WCE) were prepared from confluent HEK293 cells transiently transfected with 14 μg plasmid DNA in 10 cm tissue culture dishes. WCE supernatants were processed for IP experiments by using 2 μg primary antibodies and protein A/G mixed agarose beads (Pierce).

Statistical analysis

The χ^2 staticstic was computed manually with *P* value assigned for 1 degree of freedom in the characterization of mouse embryonic phenotype (Supplementary Table 2). For other studies, Student's two-tailed non-paired *t*-tests were carried out to determine the statistical significance of differences between samples. $P < 0.05$ was considered statistically significant for all tests.

URLs

Human Genome Browser, http://www.genome.ucsc.edu; ClustalW, http://www.ebi.ac.uk/Tools/msa/clustalw2/.

Supplementary Material

Refer to Web version on PubMed Central for supplementary material.

Acknowledgments

We thank the Marshfield Clinic Research Foundation, Center for Inherited Disease Research (supported by the US National Institutes of Health and National Heart, Lung, and Blood Institute) for genotyping support. We thank the International JSRD Study Group, E. Bertini, and the French Society of Foetal Pathology for patient referrals, J. Meerloo at the UCSD Microscopy Core (P30NS047101), T. Meerloo, Y. Jones and M. Farquhar and the CMM Electron Microscopy Core Facility at UCSD, S. Wirth and B. Willis for mutant mouse generation, C. Janke at the Institute Curie Research Center for GT335 antibody, TTLLs plasmids and technical advice, I. Drummond and N. Pathak at the Massachusetts General Hospital for *ttll6* MO, M. Gorovsky at the Univ. of Rochester for polyE and polyG antibodies, S. Audollent at the Hôpital Necker-Enfants Malades for technical help, B. Sotak, N. Akizu, A. Crawford, V. Cantagrel, and E-J. Choi for stimulating scientific discussion and comments. This work was supported by the US National Institutes of Health R01NS048453 and R01NS052455 (J.G.G.), R01DK068306 (F.H.), R01NS064077 (D.A.D.) the American Heart Association 09POST2250641 (J.E.L.), the Italian Ministry of Health (Ricerca Finalizzata Malattie Rare and Ricerca Corrente 2011), the Telethon Foundation Italy GGP08145, and the Pierfranco and Luisa Mariani Foundation (E.M.V.), Grants-in-Aid from MEXT and JSPS, #23117517 and #23570209 (K.I.), the BDF Newlife, the Medical Research Council (G0700073) and the Sir Jules Thorn Charitable Trust 09/JTA (C.A.J.), l'Agence National pour la Recherche ANR 07-MRAR-Fetalciliopathies (T.A.-B.), Simons Foundation Autism Research Initiative (J.G.G.) and the Howard Hughes Medical Institute (F.H. and J.G.G.).

References

1. Ikegami K, Sato S, Nakamura K, Ostrowski LE, Setou M. Tubulin polyglutamylation is essential for airway ciliary function through the regulation of beating asymmetry. Proc Natl Acad Sci U S A. 2010; 107:10490–5. [PubMed: 20498047]
2. Kubo T, Yanagisawa HA, Yagi T, Hirono M, Kamiya R. Tubulin polyglutamylation regulates axonemal motility by modulating activities of inner-arm dyneins. Curr Biol. 2010; 20:441–5. [PubMed: 20188560]
3. Parisi MA. Clinical and molecular features of Joubert syndrome and related disorders. Am J Med Genet C Semin Med Genet. 2009; 151C:326–40. [PubMed: 19876931]
4. Andersen JS, et al. Proteomic characterization of the human centrosome by protein correlation profiling. Nature. 2003; 426:570–4. [PubMed: 14654843]
5. van Dijk J, et al. A targeted multienzyme mechanism for selective microtubule polyglutamylation. Mol Cell. 2007; 26:437–48. [PubMed: 17499049]
6. Valente EM, Brancati F, Dallapiccola B. Genotypes and phenotypes of Joubert syndrome and related disorders. Eur J Med Genet. 2008; 51:1–23. [PubMed: 18164675]
7. Hildebrandt F, Zhou W. Nephronophthisis-associated ciliopathies. J Am Soc Nephrol. 2007; 18:1855–71. [PubMed: 17513324]
8. Lander ES, Botstein D. Homozygosity mapping: a way to map human recessive traits with the DNA of inbred children. Science. 1987; 236:1567–70. [PubMed: 2884728]
9. Yamada T, et al. The gene TSGA14, adjacent to the imprinted gene MEST, escapes genomic imprinting. Gene. 2002; 288:57–63. [PubMed: 12034494]
10. Bordo D, Bork P. The rhodanese/Cdc25 phosphatase superfamily. Sequence-structure-function relations. EMBO Rep. 2002; 3:741–6. [PubMed: 12151332]
11. Beales PL, et al. IFT80, which encodes a conserved intraflagellar transport protein, is mutated in Jeune asphyxiating thoracic dystrophy. Nat Genet. 2007; 39:727–9. [PubMed: 17468754]
12. Gorden NT, et al. CC2D2A is mutated in Joubert syndrome and interacts with the ciliopathy-associated basal body protein CEP290. Am J Hum Genet. 2008; 83:559–71. [PubMed: 18950740]
13. Colantonio JR, et al. The dynein regulatory complex is required for ciliary motility and otolith biogenesis in the inner ear. Nature. 2009; 457:205–9. [PubMed: 19043402]
14. Khanna H, et al. A common allele in RPGRIP1L is a modifier of retinal degeneration in ciliopathies. Nat Genet. 2009; 41:739–45. [PubMed: 19430481]
15. Essner JJ, Amack JD, Nyholm MK, Harris EB, Yost HJ. Kupffer's vesicle is a ciliated organ of asymmetry in the zebrafish embryo that initiates left-right development of the brain, heart and gut. Development. 2005; 132:1247–60. [PubMed: 15716348]
16. Nonaka S, et al. Randomization of left-right asymmetry due to loss of nodal cilia generating leftward flow of extraembryonic fluid in mice lacking KIF3B motor protein. Cell. 1998; 95:829–37. [PubMed: 9865700]
17. McGrath J, Brueckner M. Cilia are at the heart of vertebrate left-right asymmetry. Curr Opin Genet Dev. 2003; 13:385–92. [PubMed: 12888012]
18. Amack JD, Yost HJ. The T box transcription factor no tail in ciliated cells controls zebrafish left-right asymmetry. Curr Biol. 2004; 14:685–90. [PubMed: 15084283]
19. Ross AJ, et al. Disruption of Bardet-Biedl syndrome ciliary proteins perturbs planar cell polarity in vertebrates. Nat Genet. 2005; 37:1135–40. [PubMed: 16170314]
20. Hoover AN, et al. C2cd3 is required for cilia formation and Hedgehog signaling in mouse. Development. 2008; 135:4049–58. [PubMed: 19004860]
21. Caspary T, Larkins CE, Anderson KV. The graded response to Sonic Hedgehog depends on cilia architecture. Dev Cell. 2007; 12:767–78. [PubMed: 17488627]
22. Jurczyk A, et al. Pericentrin forms a complex with intraflagellar transport proteins and polycystin-2 and is required for primary cilia assembly. J Cell Biol. 2004; 166:637–43. [PubMed: 15337773]
23. Million K, et al. Polyglutamylation and polyglycylation of alpha- and beta-tubulins during in vitro ciliated cell differentiation of human respiratory epithelial cells. J Cell Sci. 1999; 112 (Pt 23): 4357–66. [PubMed: 10564653]

24. Suryavanshi S, et al. Tubulin glutamylation regulates ciliary motility by altering inner dynein arm activity. Curr Biol. 2010; 20:435–40. [PubMed: 20189389]
25. Vogel P, Hansen G, Fontenot G, Read R. Tubulin tyrosine ligase-like 1 deficiency results in chronic rhinosinusitis and abnormal development of spermatid flagella in mice. Vet Pathol. 2010; 47:703–12. [PubMed: 20442420]
26. Wloga D, et al. Hyperglutamylation of tubulin can either stabilize or destabilize microtubules in the same cell. Eukaryot Cell. 2010; 9:184–93. [PubMed: 19700636]
27. Becker-Heck A, et al. The coiled-coil domain containing protein CCDC40 is essential for motile cilia function and left-right axis formation. Nat Genet. 2011; 43:79–84. [PubMed: 21131974]
28. Zhao C, Malicki J. Genetic defects of pronephric cilia in zebrafish. Mech Dev. 2007; 124:605–16. [PubMed: 17576052]
29. Pathak N, Obara T, Mangos S, Liu Y, Drummond IA. The zebrafish fleer gene encodes an essential regulator of cilia tubulin polyglutamylation. Mol Biol Cell. 2007; 18:4353–64. [PubMed: 17761526]
30. Pathak N, Austin CA, Drummond IA. Tubulin tyrosine ligase-like genes ttll3 and ttll6 maintain zebrafish cilia structure and motility. J Biol Chem. 2011; 286:11685–95. [PubMed: 21262966]
31. Gaertig J, Wloga D. Ciliary tubulin and its post-translational modifications. Curr Top Dev Biol. 2008; 85:83–113. [PubMed: 19147003]
32. Shida T, Cueva JG, Xu Z, Goodman MB, Nachury MV. The major alpha-tubulin K40 acetyltransferase alphaTAT1 promotes rapid ciliogenesis and efficient mechanosensation. Proc Natl Acad Sci U S A. 2010; 107:21517–22. [PubMed: 21068373]
33. Kim SK, et al. Planar cell polarity acts through septins to control collective cell movement and ciliogenesis. Science. 2010; 329:1337–40. [PubMed: 20671153]
34. Williams CL, et al. MKS and NPHP modules cooperate to establish basal body/transition zone membrane associations and ciliary gate function during ciliogenesis. J Cell Biol. 2011; 192:1023–41. [PubMed: 21422230]
35. Rogowski K, et al. Evolutionary divergence of enzymatic mechanisms for posttranslational polyglycylation. Cell. 2009; 137:1076–87. [PubMed: 19524510]
36. Wloga D, et al. TTLL3 Is a tubulin glycine ligase that regulates the assembly of cilia. Dev Cell. 2009; 16:867–76. [PubMed: 19531357]
37. Bulinski JC. Tubulin posttranslational modifications: a Pushmi-Pullyu at work? Dev Cell. 2009; 16:773–4. [PubMed: 19531345]
38. Valente EM, et al. Distinguishing the four genetic causes of Jouberts syndrome-related disorders. Ann Neurol. 2005; 57:513–9. [PubMed: 15786477]
39. Murray SS, et al. A highly informative SNP linkage panel for human genetic studies. Nat Methods. 2004; 1:113–7. [PubMed: 15782173]
40. Hoffmann K, Lindner TH. easyLINKAGE-Plus--automated linkage analyses using large-scale SNP data. Bioinformatics. 2005; 21:3565–7. [PubMed: 16014370]
41. Inglis PN, Boroevich KA, Leroux MR. Piecing together a ciliome. Trends Genet. 2006; 22:491–500. [PubMed: 16860433]
42. Gherman A, Davis EE, Katsanis N. The ciliary proteome database: an integrated community resource for the genetic and functional dissection of cilia. Nat Genet. 2006; 38:961–2. [PubMed: 16940995]
43. Schnutgen F, et al. Genomewide production of multipurpose alleles for the functional analysis of the mouse genome. Proc Natl Acad Sci U S A. 2005; 102:7221–6. [PubMed: 15870191]
44. Valente EM, et al. Mutations in TMEM216 perturb ciliogenesis and cause Joubert, Meckel and related syndromes. Nat Genet. 2010; 42:619–25. [PubMed: 20512146]
45. Majumdar A, Drummond IA. Podocyte differentiation in the absence of endothelial cells as revealed in the zebrafish avascular mutant, cloche. Dev Genet. 1999; 24:220–9. [PubMed: 10322630]

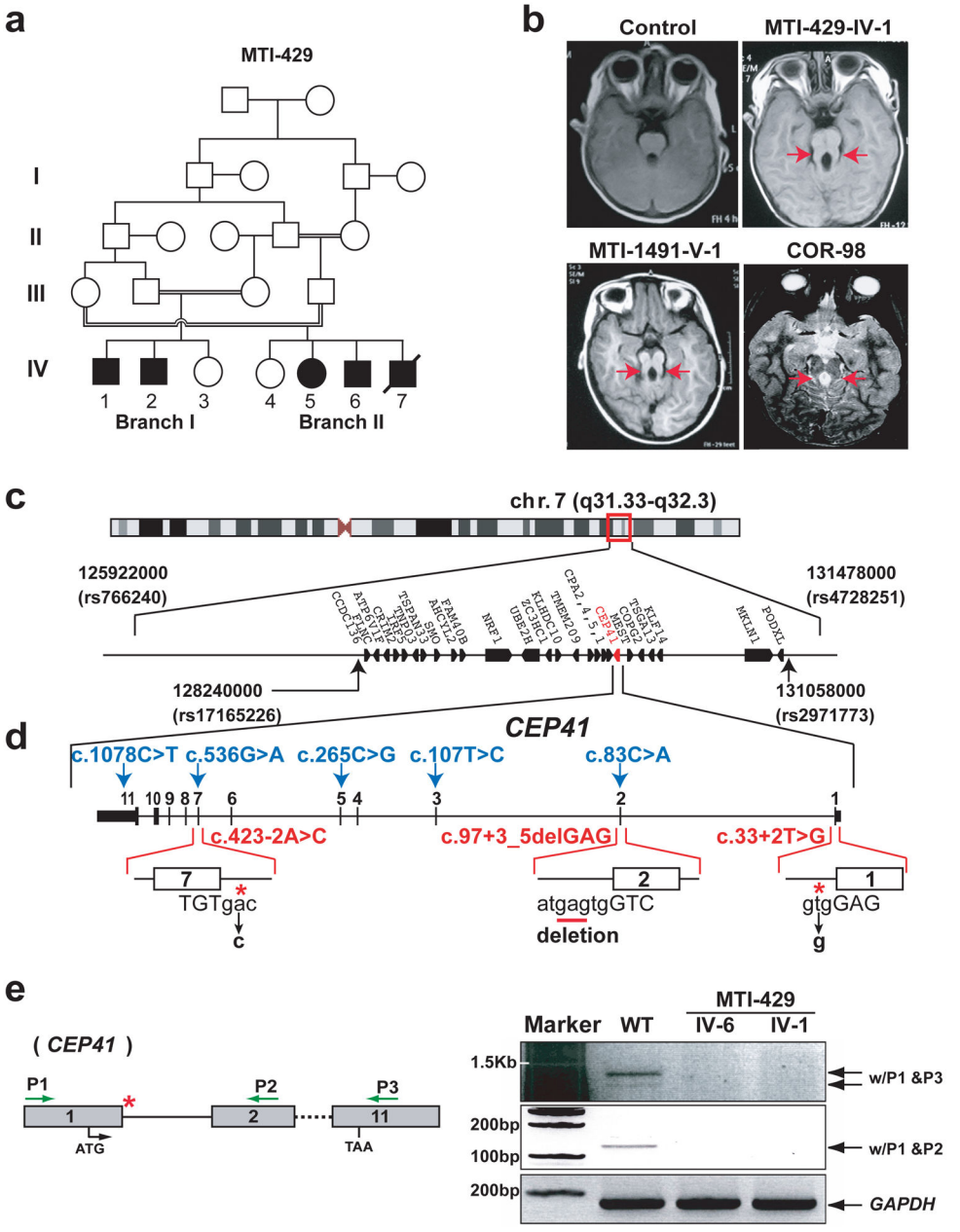

Figure 1.

Identification of mutations in *CEP41* in affected individuals linked to the JBTS15 locus. (**a**) Pedigree MTI-429 shows double first cousin marriage with five affected offspring. (**b**) Axial brain MRI images from patients with *CEP41* mutations in each MTI-429, MTI-1491 (T1-weighted) and COR-98 (T2-weighted) family, showing the 'molar tooth sign' (red arrows). (**c**) JBTS15 is 5.5 Mbp located at Chr. 7q31.33–32.3 (red box) defined by rs766240 and rs4728251. Further narrowing of the interval to 2.8 Mbp based upon denser SNP scan to encompass rs17165226 and rs2971773 (black arrows). (**d**) *CEP41* genomic organization, depicting locations of identified base changes including homozygous (red) splice mutations and heterozygous (blue) missense or nonsense mutations. Capital letters: exon sequences,

small letters: intron sequences, asterisks: point mutations, underline: deletion. (**e**) RT-PCR confirmation of the splicing defect of *CEP41* in MTI-429 patient fibroblasts. Both *CEP41* mutant cells failed to produce *CEP41* mRNA, compared with WT. GAPDH is control. Green arrows: positions of primers, asterisk: region of splice mutation in MTI-429.

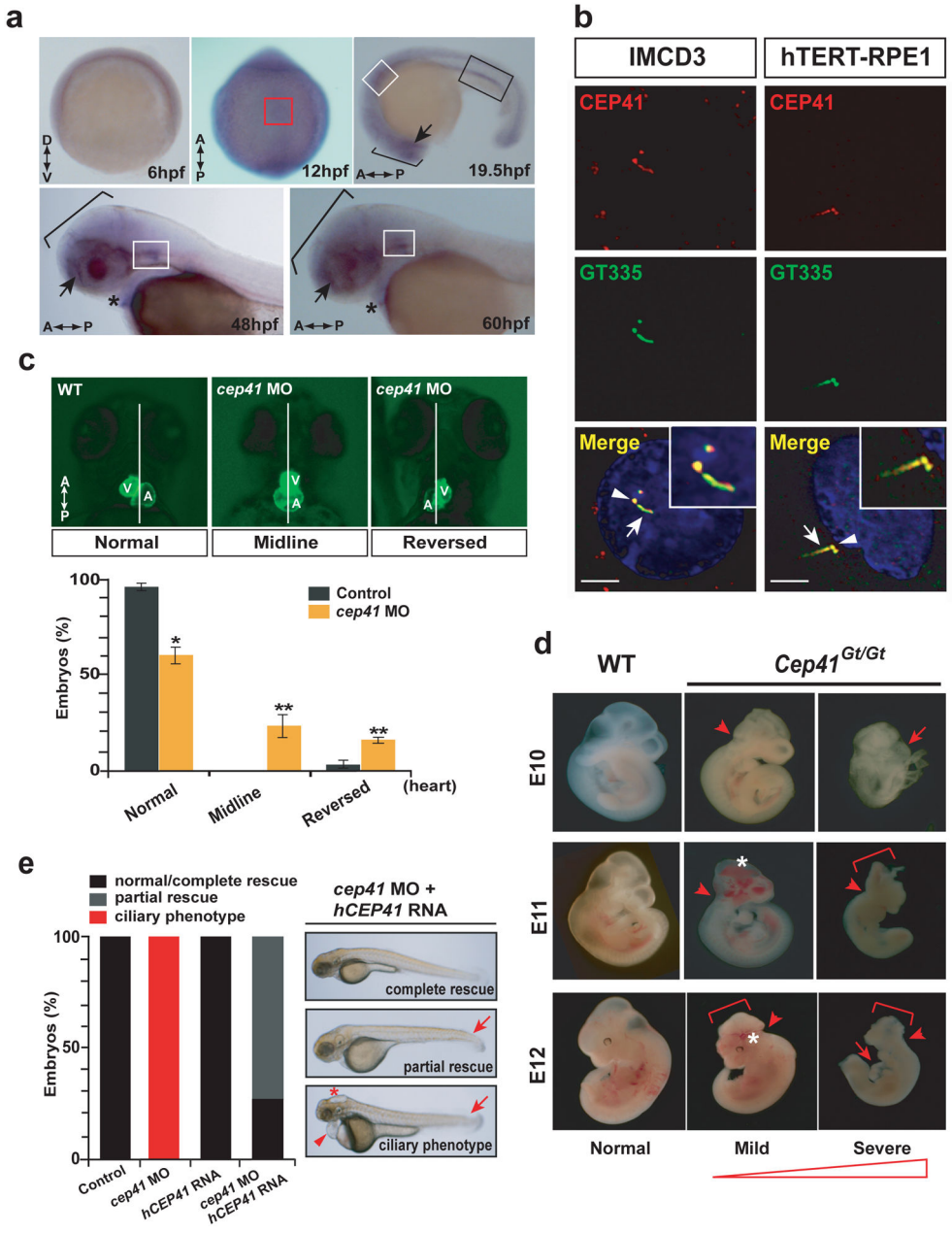

Figure 2.

CEP41 is expressed in ciliated tissues and its loss recapitulates ciliopathy-related phenotypes in zebrafish and mouse. (**a**) Zebrafish *cep41* mRNA is expressed ubiquitously at gastrulation stages (6 hpf), but at later stages, it is specifically expressed in ciliated organs: Kupffer's vesicle (red box), inner ear (white boxes), brain (brackets), eyes (arrows), pronephric duct (black box), and heart (asterisks). A, anterior; D, dorsal; P, posterior; V, ventral. (**b**) CEP41 is predominantly localized to the basal body (arrowheads) and primary cilium (arrows) in ciliated IMCD3 and hTERT-RPE1 cells. Insets: co-localization of CEP41 with GT335, a marker of basal bodies and cilia. Scale bar 5 μm. (**c**) Knockdown of *cep41* by injection of morpholino oligonucleotide (MO) causes heart asymmetry defects in Tg

(*myl7:egfp*) zebrafish embryos. The *cep41* morphants show either loss of asymmetry (midline) or inversion of V/A asymmetry (reversed) at 72hpf. **P* < 0.01, ***P* < 0.001. Error bars: s.e.m. A, atrium; L, left; R, right; V, ventricle. (**d**) Murine *Cep41* gene-trap shows altered embryonic morphogenesis. Range of phenotypes of $Cep41^{Gt/Gt}$ embryos includes mild malformed hindbrain (arrowheads), exencephaly (brackets), hemorrhage in the head (asterisk), dilated pericardial sac (arrows), failure to rotate and lethality at E10–12. (**e**) Injection of human *CEP41* RNA into *cep41* morphants rescued ciliary phenotypes of pericardial edema (arrowhead), hydrocephalus (asterisk) and curved tail (arrow), completely or partially.

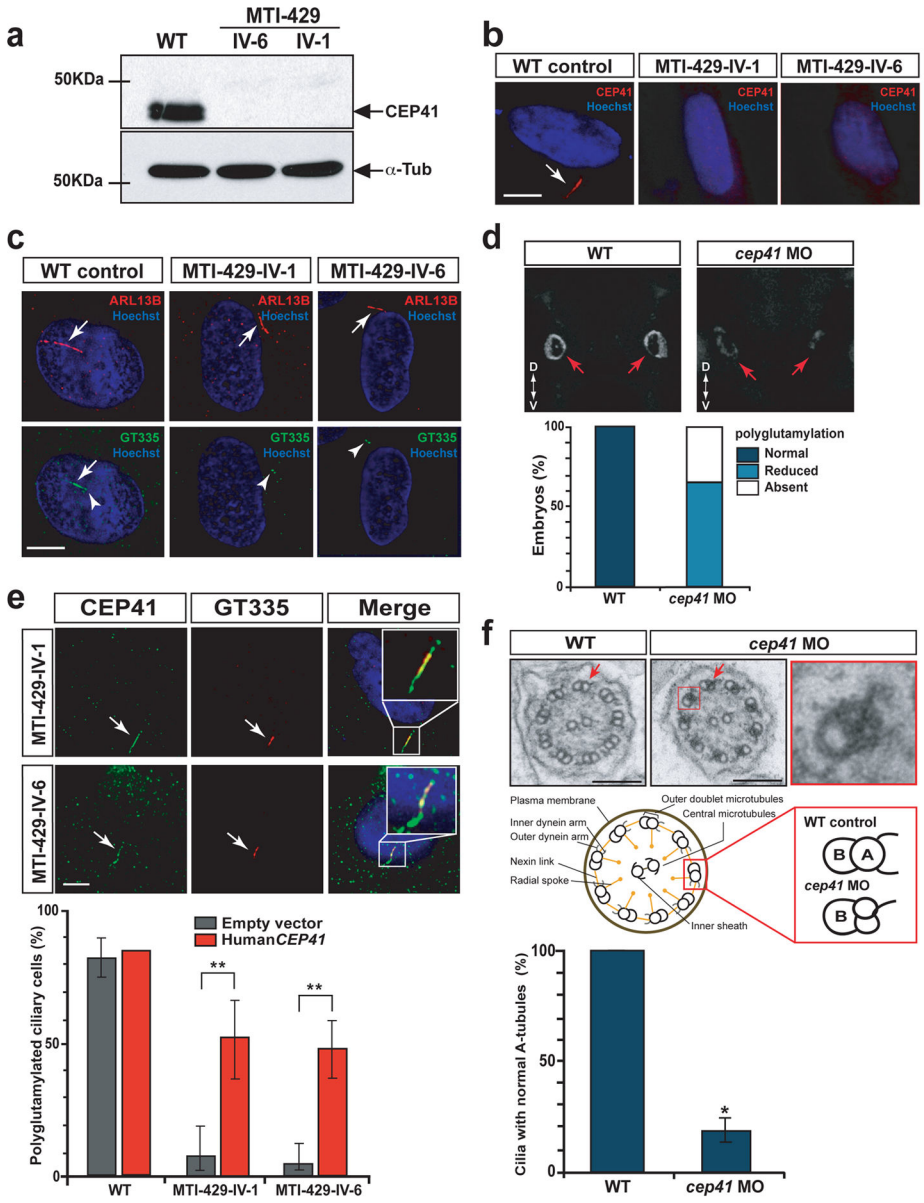

Figure 3.

CEP41 is required for tubulin glutamylation at the ciliary axoneme. (**a**) Absent CEP41 protein in *CEP41* mutant patient cells. (**b**) Ciliary localization of endogenous CEP41 in human fibroblasts and loss of the protein in *CEP41* mutant cilia. Scale bar 5 μm. (**c**) WT cells have both GT335-positive basal bodies (arrowheads) and cilia (arrows, marked by ARL13B), while mutant cells show staining of GT335 only at the basal bodies. Scale bar 5 μm. (**d**) Depletion of *cep41* causes glutamylation defects in zebrafish olfactory placode cilia (red arrows). Images of GT335-stainined WT and *cep41* morphant embryos were taken in anterior view (head is up and tail is down, D, dorsal; V, ventral), quantified below. (**e**) Exogenous *CEP41* expression restores ciliary axoneme glutamylation in *CEP41* mutant cells. Arrows: primary cilia stained for CEP41 and GT335. Insets: merged images at higher power, quantified below. Scale bar 5 μm. $^{**}P < 0.001$; error bars = s.e.m. (**f**) Ultrastructural

analysis of the pronephric ciliary axoneme at 72 hpf zebrafish embryos. Compared to WT, *cep41* morphants have A-tubule specific defects in the outer doublet microtubules. Arrows: A-tubules and one of nine outer doublet microtubules is magnified in the red box. The numbers of cilia, categorized in normal and abnormal A-tubules according to the schematic, were counted in both WT embryos and *cep41* morphants (n = 3 embryos, >20 cilia per animal), quantified below. Scale bar 100 nm. $^{**}P < 0.01$; error bars = s.e.m.

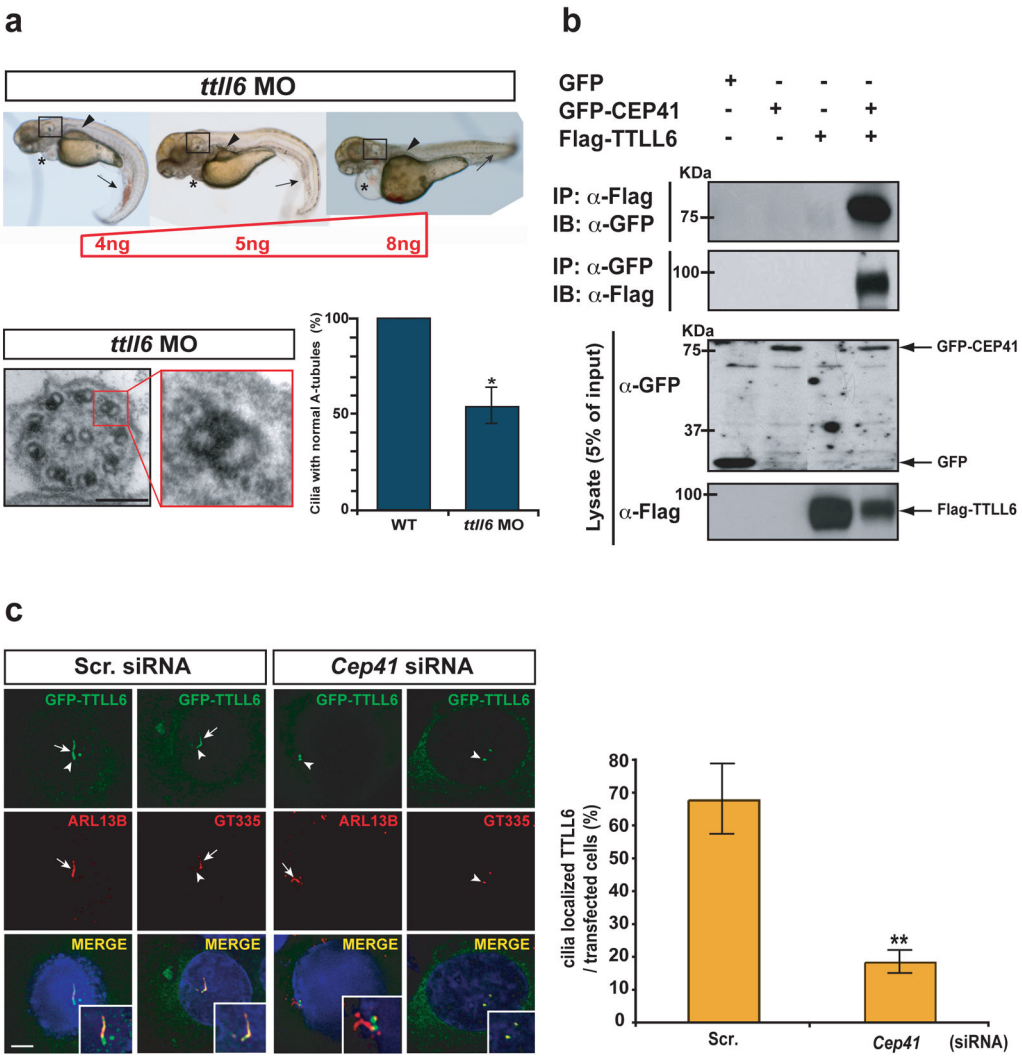

Figure 4.

CEP41 interacts with TTLL6 and is required for localizing TTLL6 to the cilium. (**a**) Morpholino knockdown of zebrafish *ttll6* associates with ciliary phenotypes such as curved tail (arrows), abnormal number/orientation of ear otolith (boxes), cystic kidney (arrowheads) and peripheral cardiac edema (asterisks) at different dosages indicated and show A-tubule specific defects in the outer doublet microtubules. The numbers of defective cilia were counted in both WT embryos and *ttll6* morphants (n = 3 embryos, >20 cilia per animal), quantified below. (**b**) GFP-CEP41 was immunoprecipitated with anti-Flag antibody recognizing Flag-tagged TTLL6 from whole-cell extract (WCE), compared with GFP-empty vector. In the reciprocal co-IP experiment with anti-GFP antibody, the interaction between CEP41 and TTLL6 was confirmed. (**c**) Disturbed localization of TTLL6 to the cilium following *Cep41* siRNA co-transfection with GFP-TTLL6 into IMCD3 cells and immunostained with either GT335 or ARL13B antibody. Arrows: cilia; Arrowheads: basal bodies. Cells expressing ciliary localized TTLL6 were counted only in siRNA-transfected cells quantified in graph. Scale bar 5 μm. *P< 0.01, **P < 0.001. Error bars = s.e.m.

Table 1

Abbreviations. AG: Ambiguous genitalia, B: Bilateral, F: Female, GHD: Growth hormone deficiency, M: Male, MP: Micropenis, N: No, N/A: Not available/Not applicable, NPHP: Nephronophthisis, OMA: oculomotor arpaxia, PDSV: potentially deleterious sequence variant, UCD: Urinary concentration defect, U: Unilateral, Y: Yes

Demographic Information								
Family ID	**MTI-429-IV-1**	**MTI-429-IV-2**	**MTI-429-IV-5**	**MTI-429-IV-6**	**MTI-429-IV-7**	**MTI-1491-V-2**	**MTI-1491-V-3**	**COR-98**
Country of orgin	Egypt	Egypt	Egypt	Egypt	Egypt	Egypt	Egypt	Portugal
Patient (sex)	M	M	F	M	M	F	F	M
Death	N	N	N	N	died at 7 days	N	N	N
Documented Consanguinity	Y	Y	Y	Y	Y	Y	Y	Y
Neurological signs								
Hypotonia/Ataxia	Y	Y	Y	Y	Y	Y	Y	Y
Psychomotor Delay	Y	Y	Y	Y	N/A	Y	Y	Y
Mental Retardation	mild	borderline	borderline	borderline	N/A	Y	Y	Y
OMA	Y	Y	N	N	N/A	Y	Y	N
Breathing Abnormalities	N	N	N	N	Y	Y	Y	N
Head Circumference	50%ile	50%ile	50%ile	50%ile	75%ile	50%ile	50%ile	N/A
Ocular Signs								
Retinopathy	N	N	N	N	U	N	N	Y
Other abnormalities	B ptosis	U ptosis and leukoma	U ptosis	N	N	U ptosis, squint, leukoma	B squint and leukoma	N
Coloboma	N	N	N	N	U	N	N	N
Renal signs								
NPHP/UCD	N	N	N	N	U	N	N	N
Kidney ultrasound	N	N	N	N	N	N	N	N
Other organs								
Liver abnormalities	N	N	N	N	M	N	N	N
Polydactyly	N	N	U postaxial	U postaxial	B postaxial	N	U postaxial	Y
Other abnormalities	GHD, MP	GHD, MP	N	MP	AG, MP, hypoplastic scrotum	N	N	N

Demographic Information								
Family ID	**MTI-429-IV-1**	**MTI-429-IV-2**	**MTI-429-IV-5**	**MTI-429-IV-6**	**MTI-429-IV-7**	**MTI-1491-V-2**	**MTI-1491-V-3**	**COR-98**
MRI reading								
MTI	Y	Y	Y	Y	Y	Y	Y	Y
Other abnormalities	N	N	N	N	N	N	N	N
***CEP41* mutation analysis**								
exon(s)	1					2		7
Hetero/Homozygous	Homozygous					Homozygous in JS		Homozygous
Nucleotide change	c.33+2T>G					c.97+3_5delGAG		c.423-2A>C
Amino acid change	Splice					Splice		Splice
Amino acid consequence	Premature stop					Premature stop		Predicted Premature stop
Comprehensive JSRD Geneti Screening								
Linkage	Linkage chr7 (q31.33–q32.3)					Linkage negative to *AHI1, TMEM67-, TMEM138/216-*		Linkage negative to *AHI1, TMEM67-, TMEM138/216-*
Additional gene with PDSV	None					None		*CEP290*
exon								31
Hetero/Homozygous								Heterozygous
Nucleotide change								c.3626C>G
Amino acid change								p.1209S>C
Amino acid consequence								Neutral to neutral
In NCBI SNP Database								No